Hassan Javed, Mohammad Islam*, Nasir Mahmood, Amine Achour, Asad Hameed and Nasrullah Khatri

Catalytic growth of multi-walled carbon nanotubes using $NiFe_2O_4$ nanoparticles and incorporation into epoxy matrix for enhanced mechanical properties

Abstract: Mechanical properties of multi-walled carbon nanotubes (CNT) reinforced epoxy nanocomposites, with and without any structural defect, were investigated using different weight percent values of pristine and covalently functionalized CNT. First, nickel ferrite ($NiFe_2O_4$) catalyst nanoparticles were prepared using the co-precipitate method followed by CNT growth via chemical vapor deposition, using acetylene as carbon feedstock. Through a combination of magnetic stirring and ultrasound vibration treatments in acetone, pristine, COOH-, or NH_2-functionalized CNTs at 0.15, 0.60, 1.10 and 1.50 wt% were added to the Epon 828 epoxy. During each stage, extensive materials characterization was carried out using scanning electron microscopy (SEM), transmission electron microscopy (TEM), X-ray diffraction (XRD), Fourier transform infrared (FTIR) and thermogravimetric analysis (TGA)/differential thermal analysis (DTA) techniques. Tensile testing of the specimens revealed an increase in the elastic modulus and tensile strength values with maximum increase registered in the case of nanocomposites made from 1.1 wt% CNT-NH_2 (+73%) or CNT-COOH (67%) addition. The energy absorbed during impact testing also increased by 86% upon addition of 1.50 wt% CNT-NH_2. The presence of a small notch in the nanocomposite specimens yielded superior mechanical properties to those of the neat epoxy. Such enhancement in the mechanical properties can be attributed to better CNT dispersion in the nanocomposites and good interfacial bonding, as confirmed from microstructural examination of the fractured surfaces.

Keywords: carbon nanotubes; covalent functionalization; epoxy; ferrite nanoparticles; nanocomposites; solution mixing.

DOI 10.1515/polyeng-2015-0137
Received February 4, 2015; accepted April 20, 2015

***Corresponding author: Mohammad Islam,** Center of Excellence for Research in Engineering Materials (CEREM), Advanced Manufacturing Institute, King Saud University, P.O. Box 800, Riyadh 11421, Saudi Arabia, e-mail: mohammad.islam@gmail.com. http://orcid.org/0000-0003-0117-6422
Hassan Javed: School of Chemical and Materials Engineering, National University of Sciences and Technology, Islamabad, Pakistan; and Department of Materials Science and Engineering, University of Erlangen Nuremberg, Martensstr. 5–7, Erlangen 91058, Germany
Nasir Mahmood: School of Chemical and Materials Engineering, National University of Sciences and Technology, Islamabad, Pakistan; and Department of Materials Science and Engineering, College of Engineering, Peking University, Beijing 100871, China
Amine Achour: Laboratoire d'Analyse et d'Architecture des Systèm (LAAS), CNRS, 7 Avenue du Colonel Roche, 31400 Toulouse, France; and Institut des Matériaux Jean Rouxel (IMN), Université de Nantes, CNRS, 2 rue de la Houssinière, BP 32229, 44322 Nantes Cedex3, France
Asad Hameed: Department of Materials, University of Oxford, 16 Parks Road, OX1 3PH, Oxford, UK
Nasrullah Khatri: School of Chemical and Materials Engineering, National University of Sciences and Technology, Islamabad, Pakistan

1 Introduction

Carbon nanotubes (CNT) have attracted the attention of researchers all over the world because of their remarkable structural, mechanical, electrical, and thermal properties [1, 2]. Multi-walled CNT that are comprised of several coaxial shells of rolled graphene sheets, offer unique properties with potential for applications in various fields of science [3, 4]. Among several CNT synthesis routes, catalytic chemical vapor deposition has advantages of higher purity and yield despite the cost factor associated with this technique [5]. It is also a relatively simple, economical, and easy to scale-up method that has been widely adopted, because of its ability to produce large amounts with high purity and the ease of controlling reaction conditions to produce the desired type of carbon

nanostructures. There are several reports on the effects of different processing parameters, including reaction time, amount of catalyst nanoparticles (in terms of size or area density), precursor gas flow rate and composition, chamber pressure, etc. on certain attributes of the CNTs [6–19].

In most cases, CNT incorporation into a matrix material requires a post-synthesis purification step for removal of catalyst nanoparticles and other carbonaceous deposits. From a practical viewpoint, therefore, it is desirable that CNT with high purity and narrow size distribution (outer diameter) are produced in high yield. Certain issues inherent to polymer matrix reinforcement with CNT are agglomeration due to extremely large specific surface area and strong van der Waals forces, inhomogeneous distribution and little or no chemical affinity of CNT towards the matrix. Such challenges can be addressed through CNT surface modification via physical or chemical attachment of different functional groups. Although acid treatment removes catalyst nanoparticles beside attachment of carboxyl (-COOH) groups to the nanotubes [20–22], the external CNT shells get damaged due to the action of these acids. To ensure strong interfacial strength between CNT and the matrix, further treatment of oxidized multi-walled CNT to attach amine groups is necessary.

Epoxy-based composites find extensive applications in the aerospace industry, space shuttle and many other industries because of high strength and light weight. The utilization of epoxy resin as matrix material has drastically increased due to its good engineering properties, namely resistance to creep, inertness to chemical attack, high stiffness and strength, and strong adhesion to many substrates, although its use has been associated with drawbacks of brittleness, tendency to delaminate and low fracture toughness after curing. A recent approach towards overcoming these issues, without sacrificing other important properties, is epoxy reinforcement with nanostructures in the form of nanoparticles or nanotubes [23–25]. It has been reported that properties of several polymer matrices improve significantly upon reinforcement with nanostructures at volume fractions as low as 0.1 wt%, primarily due to high surface-area-to-volume ratio and aspect ratio of these one-dimensional materials [26–29].

Although CNT-reinforced epoxy nanocomposites are among the promising advanced materials, several challenges are encountered in the process of achieving the promised properties: (i) due to high aspect ratio and greater van der Waals forces, CNT tend to agglomerate, thus forming bundles when poured inside the matrix; (ii) CNT have low solubility in either organic or inorganic solvents that makes uniform dispersion difficult to achieve; and (iii) relatively low chemical reactivity of the CNT due to their aromatic structure causes poor interfacial interactions [27]. For uniform dispersion, various physical treatments (ball milling, stirring, calendaring, ultra-sonication, extrusion) or chemical treatments (CNT outer surface modification via processes like oxidation, halogenation, hydrogenation or reaction with the polymers) can be employed with certain merits and demerits associated with each approach [27, 30].

In an attempt to develop CNT-reinforced epoxy nanocomposites, we first prepared nickel ferrite ($NiFe_2O_4$) nanoparticles through surfactant-assisted control on size distribution, followed by CNT growth using a mixture of acetylene (C_2H_2) as a carbon feed stock and argon gas for dilution purposes. Pristine as well as functionalized CNT were added to the epoxy to obtain nanocomposites with 0.15–1.50 wt% loadings. The $NiFe_2O_4$ nanoparticles, as-synthesized as well as functionalized CNT, were characterized for composition and morphology using scanning electron microscopy (SEM) and transmission electron microscopy (TEM). Thermal stability of the CNT and nanocomposites was assessed through thermogravimetric analysis (TGA)/differential thermal analysis (DTA) studies. The results from tensile and impact testing of the specimens and microstructural examination of the fractured surfaces are presented and discussed.

2 Materials and methods

The chemicals and liquids used for this study (>99.9% or higher purity) were procured from Sigma Aldrich (Hong Kong, China) and used without any further treatment. The experimentation phase spanned over four stages, starting from synthesis of $NiFe_2O_4$ nanoparticles via the co-precipitate method followed by growth of multi-walled CNTs and their functionalization. Different wt% of the pristine or chemically modified nanotubes were subsequently incorporated into commercially available diglycidyl ether of bisphenol-A (EPON 828, Shell Chemical Company, Houston, TX, USA) and 4,4′-diaminodiphenyl sulfone as curing agent, followed by tensile and impact testing of the nanocomposite specimens.

2.1 $NiFe_2O_4$ nanoparticles synthesis

Using the co-precipitate method, $NiFe_2O_4$ catalyst nanoparticles were prepared in the aqueous medium using sodium hydroxide (NaOH) as precipitating agent and cetyltrimethylammonium bromide (CTAB) as a surfactant

to control the size and distribution of nanoparticles. The step-by-step procedure is described as follows: aqueous solutions of nickel chloride ($NiCl_2$) and ferric chloride [$Fe(NO_3)_3$] salts were prepared separately by dissolving 0.1 M $NiCl_2$ (2.38 g $NiCl_2{\cdot}6H_2O$) and 0.2 M $Fe(NO_3)_3$ [8.04 g $Fe(NO_3)_3{\cdot}9H_2O$] in 100 ml double-distilled water and vigorously stirred at 75°C. Both solutions were mixed, followed by addition of 18.3 g CTAB (0.5 M) aqueous solution and stirring at 80°C. The resulting solution was added to a 3.0 M NaOH solution, made by dissolving 12 g NaOH in 100 ml water and continuously stirring at 75°C. The pH value of the solution mixture was maintained at 13 with the help of NaOH. After 1 h, the solution was cooled down, washed for five times with water and dried overnight at 100°C.

2.2 CNT growth and functionalization

A suspension of $NiFe_2O_4$ catalyst particles was made in ethanol (C_2H_5OH) through ultrasonic vibration for 2 h. A few drops out of the suspension were taken over silicon and the substrates loaded with catalyst nanoparticles were transferred to the tube furnace and heated to 680°C at 10°C/min. At this temperature, argon gas flow was maintained for 15 min followed by introduction of C_2H_2 and argon gas mixture at flow ratio (standard cubic centimeter or sccm) of 1:7, 1:8 or 1:9 for 24, 27 or 30 min. Dilution of C_2H_2 gas with argon prevents excess supply of carbon feedstock to the catalyst, formation of excessive soot and oxidation of carbon at high temperature.

After synthesis, CNT were refluxed in 37% (v/v) HCl at 110°C for 6 h to remove catalyst nanoparticles followed by deionized water wash and filtration. Any organic residue and other carbonaceous materials were removed through CNT heat treatment at 400°C for 3 h. The purified CNT were added to the HNO_3:H_2SO_4 solution (1:3 w/w) and dispersed through ultrasonic vibration for 2 h and then refluxed at 85°C for 12 h. Besides attachment of hydroxyl (-OH) and carboxyl (-COOH) groups to CNTs, such acid treatment introduces defects on nanotubes sidewalls and shortens CNT length. The acid residues were subsequently removed by washing CNTs with deionized water until solution pH became ~7. After filtration through microporous membranes, the functionalized CNT were dried in oven at 110°C for 12 h and heat treated at 350°C for 30 min to remove traces of any acids. The chemical reaction of acid treated CNT with excess thionyl chloride in the form of sonication for 10 min and then a refluxing reaction at 50–60°C for 24 h, resulted in attachment of acyl group to the nanotubes. The residual $SOCl_2$ was removed by distillation under reduced pressure. Excess amount of $SOCl_2$ was removed from CNT by washing with anhydrous tetra-hydrofuran followed by drying at 60°C to yield acyl-functionalized CNT. Attachment of amine group was accomplished through ultrasonic treatment of acyl-functionalized CNT in ethylenediamine (EDA) for 6 h followed by refluxing at 85°C for 18 h. Excess EDA was distilled under vacuum. After that, CNT-NH_2 was washed with anhydrous C_2H_5OH to remove the residual EDA and dried at 70°C. Throughout this paper, purified, carboxyl-, acyl- and amine-functionalized CNT will be referred to as CNT-Pristine, CNT-COOH, CNT-OCl and CNT-NH_2, respectively.

2.3 Preparation of epoxy/CNT nanocomposites

Epoxy CNT composites were prepared using the solution mixing process. Different batches with varying amounts of pristine and functionalized CNT from 0.15 wt% to 1.50 wt% were manufactured. A certain amount of CNT was added in small amounts to acetone in the presence of magnetic stirring at 500 rpm. The CNT dispersion was further ensured through ultrasound treatment at room temperature for 40 min. In a separate beaker, part A resin (epoxy) was taken and heated to 60°C for 5 min in order to lower its viscosity. The CNT/acetone solution was added to the heated epoxy resin and the resulting mixture was stirred for 2 h at 500 rpm followed by 1.5 h sonication at 60°C. The solvent (acetone) was evaporated from the solution mixture by heating at 80°C for 30 min, while the mixture was stirred at 100 rpm. At that stage, the hardener (part B) was added (35 wt% of the epoxy) to the well-dispersed CNTs suspension in epoxy resin (part A) and then stirred at 500 rpm for 5 min.

Two types of test samples, i.e., tensile and impact, were prepared for characterization. For that purpose, the mixture was initially placed in a desiccator connected to vacuum oven for 10 min to remove air bubbles and solvent, if present. In a horizontally balanced, preheated steel mold with inner surfaces coated with a mold release agent, the CNT/epoxy mixture was poured and cured first at 80°C for 1 h and then at 140°C for 2 h. After extraction from the mold, the specimens were mildly ground to obtain smooth, flat surfaces.

2.4 Materials characterization and mechanical testing

Microstructure and morphology of mixed ferrite nanoparticles and CNT was carried out using a scanning electron microscope (SEM) (JEOL JSM 6460) and a high-resolution

transmission electron microscope (HR-TEM) (Hitachi HNAR9000). Phase and crystallite size analysis of the catalyst nanoparticles, as well as assessment of chemical functionalization of CNTs, were performed using an X-ray diffractometer (XRD) (STOE Stadi MP). Thermal analysis of mixed ferrites, pristine and functionalized CNTs was done by operating a thermogravimetric analyzer (TGA) (TA Instruments Pyris 1 diamond Q5000IR) at a rate of 10°C/min. Attachment of various functional groups to CNT surface was assessed by means of using attenuation-total-reflection, Fourier transform infrared spectroscopy (ATR-FTIR) (JASCO FTIR-4100). Defect functionalization of CNTs was investigated using an FT Raman spectrometer (Bruker RFS 100, France) using an excitation wavelength of 1064 nm.

During mechanical testing, the specimens for tensile testing were produced according to ASTM 638 type 1 at different volume fractions of pristine and functionalized CNTs. Two types of tensile samples were manufactured: notch free and with small notch (~0.3 mm) at the bottom. The specimens for impact tests were made in accordance with the ASTM A370 using the same fraction of reinforced CNTs as those for tensile specimens. Tensile tests of the prepared samples were performed at 5 mm/min rate using a composite tensile testing machine (AG-X Plus model), whereas the impact tests were carried out using the Charpy impact testing method.

3 Results and discussion

3.1 $NiFe_2O_4$ catalyst nanoparticles

The results from microstructural and compositional characterization of the $NiFe_2O_4$ nanoparticles, used to catalyze CNT growth, are presented in Figure 1. The main attributes

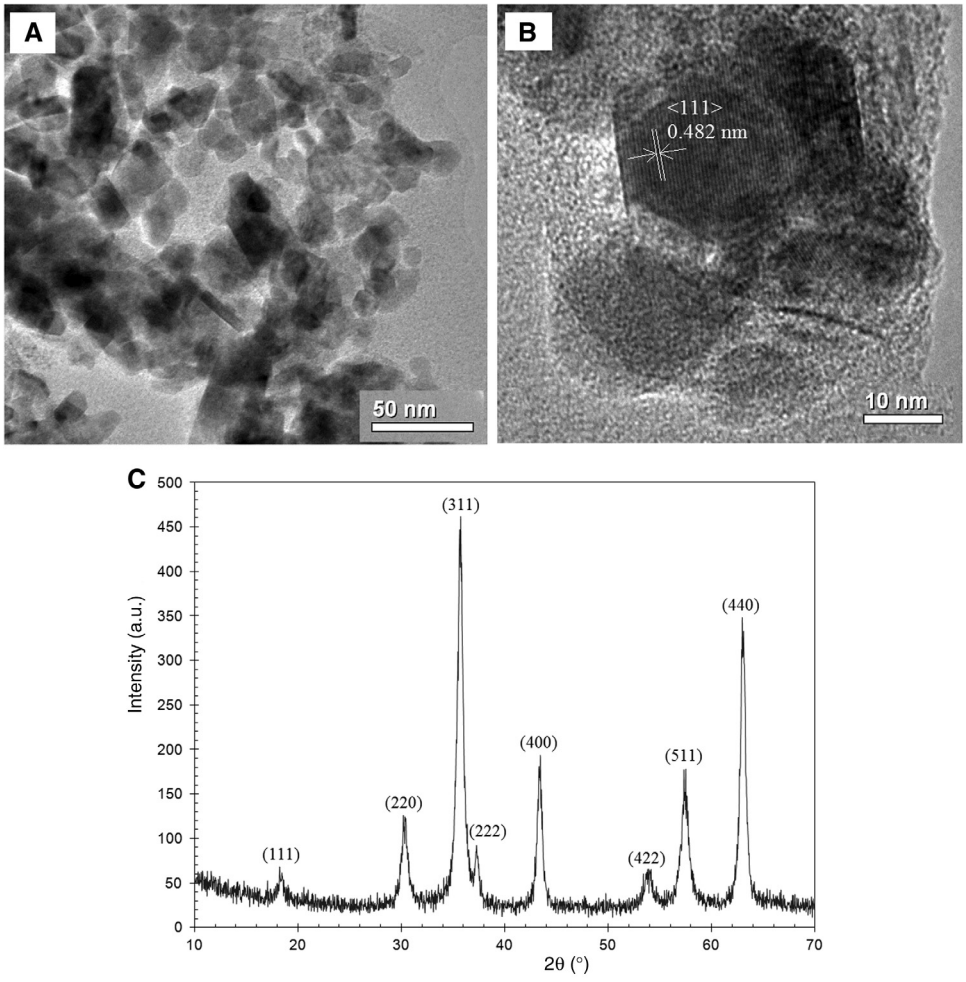

Figure 1: Morphological and composition analysis of $NiFe_2O_4$ nanoparticles: (A, B) low magnification and high-resolution transmission electron microscopy (TEM) microstructures and (C) X-ray diffraction pattern.

of the catalyst nanoparticles, namely average size and size distribution, have significant effects on the outer diameter and aspect ratio of the CNT. The cationic surfactant CTAB is a quaternary ammonium compound with bromide as a counter ion. It is completely soluble in water and is not sensitive to pH. During nanoparticles synthesis, the use of an appropriate surfactant reduces and controls nanoparticles size by capping the nanoparticles formed, thus curbing their tendency to agglomerate, as well as narrowing the particle size distribution [31, 32]. As shown in Figure 1A, the low magnification TEM microstructure of the nanoparticles reveals spherical structural morphology with an average particle size of 14±3 nm, although particles <10 nm in size are also present. The lattice fringes evident from HR-TEM examination, presented in Figure 2B, indicate {111} plane with the lattice spacing of 0.485 nm, thereby confirming a cubic spinel structure of the $NiFe_2O_4$ nanoparticles.

The XRD pattern (Figure 1C) exhibits diffraction peaks that can be indexed to be due to (111), (220), (311), (222), (400), (422), (511) and (440) reflection planes. The results indicate spinel cubic structure of the composition $NiFe_2O_4$ (JCPDS file no. 54-0964). For the most intense diffraction peak representative of (311), the crystallite size (t) as determined from the Scherrer equation $t=0.94\,\lambda/\beta\,\cos\theta$, was computed to be 16 nm, which is in agreement with TEM observations.

The weight loss data over the measured range of temperatures, obtained from TGA (Figure 2A), indicates that upon heating from room temperature to 750°C, the sample weight was reduced to approximately 70% of its initial value. About 9% weight loss which occurred upon heating to 140°C is attributed to evaporation of the absorbed water from the sample. A further drop in the sample weight to 76% maybe be attributed to the decomposition and oxidation of CTAB surfactant used to control nanoparticles size. From differential thermal analysis (DTA) data shown graphically in Figure 2B, the broad exothermic peak in the 340–390°C temperature range signifies the occurrence of a solid state reaction between α-Fe_2O_3 and NiO phases to form mixed $NiFe_2O_4$. Another exothermic peak at 462°C is due to the presence of trace NiO in the $NiFe_2O_4$-NiO phase mixture [33]. Thus, TGA studies depict the CNT growth temperatures to be in the 600–700°C regime where catalyst nanoparticles are stable.

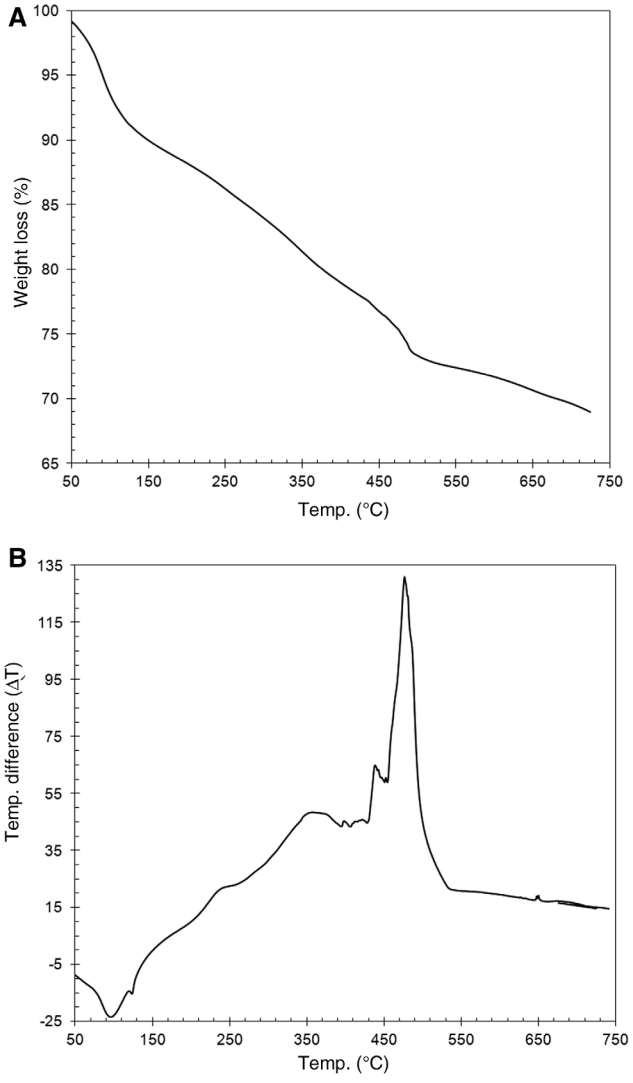

Figure 2: (A) Thermogravimetric (TG) and (B) differential thermal analysis curves for $NiFe_2O_4$ nanoparticles.

3.2 Pristine and functionalized CNT

The processing conditions for CNT growth, namely, C_2H_2:argon flow ratio and deposition time at 680°C, were optimized to obtain a high yield with narrow distribution of outer diameter. Whereas pure C_2H_2 flow or dilution with argon gas to a certain extent causes poisoning of the catalyst nanoparticles through complete encapsulation by carbonaceous forms, further C_2H_2 gas dilution initially promotes synthesis of thick nanotubes/nanofibers with a low aspect ratio and high soot content. In our case, the C_2H_2:argon ratio of 1:9 and growth time of 24 min produced randomly oriented multi-walled CNT with high purity and yield. After heat treatment at 400°C under atmospheric conditions to remove carbon soot by oxidation, acid treatment was carried out for further purification and modification of CNT outer surface, breaking the side-wall neutrality and attachment of -COOH and -NH_2 functional groups. The functionalized moieties prevent CNT from agglomeration owing to high steric hindrance,

thus providing an opportunity to tailor nanocomposites with homogenous CNT dispersion.

The microstructures of the pristine and acid-treated nanotubes as examined under electron microscopes are given in Figure 3. In the absence of any mechanism responsible for alignment during growth, the CNT growth occurs in a random fashion with a spaghetti-like appearance (Figure 3A). The average values of the CNT outer diameter and length are about 25 nm and a few micrometers, respectively, with an estimated aspect ratio of ≥40. A few of the pristine CNTs entangled with each other are presented in Figure 3B, with the inset showing an elongated nanoparticle trapped inside an individual CNT, confirming its role towards catalytic synthesis of CNT as well as the dependence of CNT outer diameter on the nanoparticle size. During the initial phase of C_2H_2 precursor gas flow, the hydrogen generated from pyrolytic decomposition of C_2H_2 causes reduction of $NiFe_2O_4$ nanoparticles to NiFe based alloy composition, with an associated decrease in the nanoparticle size. The CNT growth temperature also softens the nanoparticle, causing a change from an initial spherical to cylindrical shape. The multi-shell CNT structure is evident from diffraction fringes observed at high magnification, shown in Figure 3D. The effect of acid treatment on impurity removal and damage induced in terms of distortion in the linearity of the multi-walled

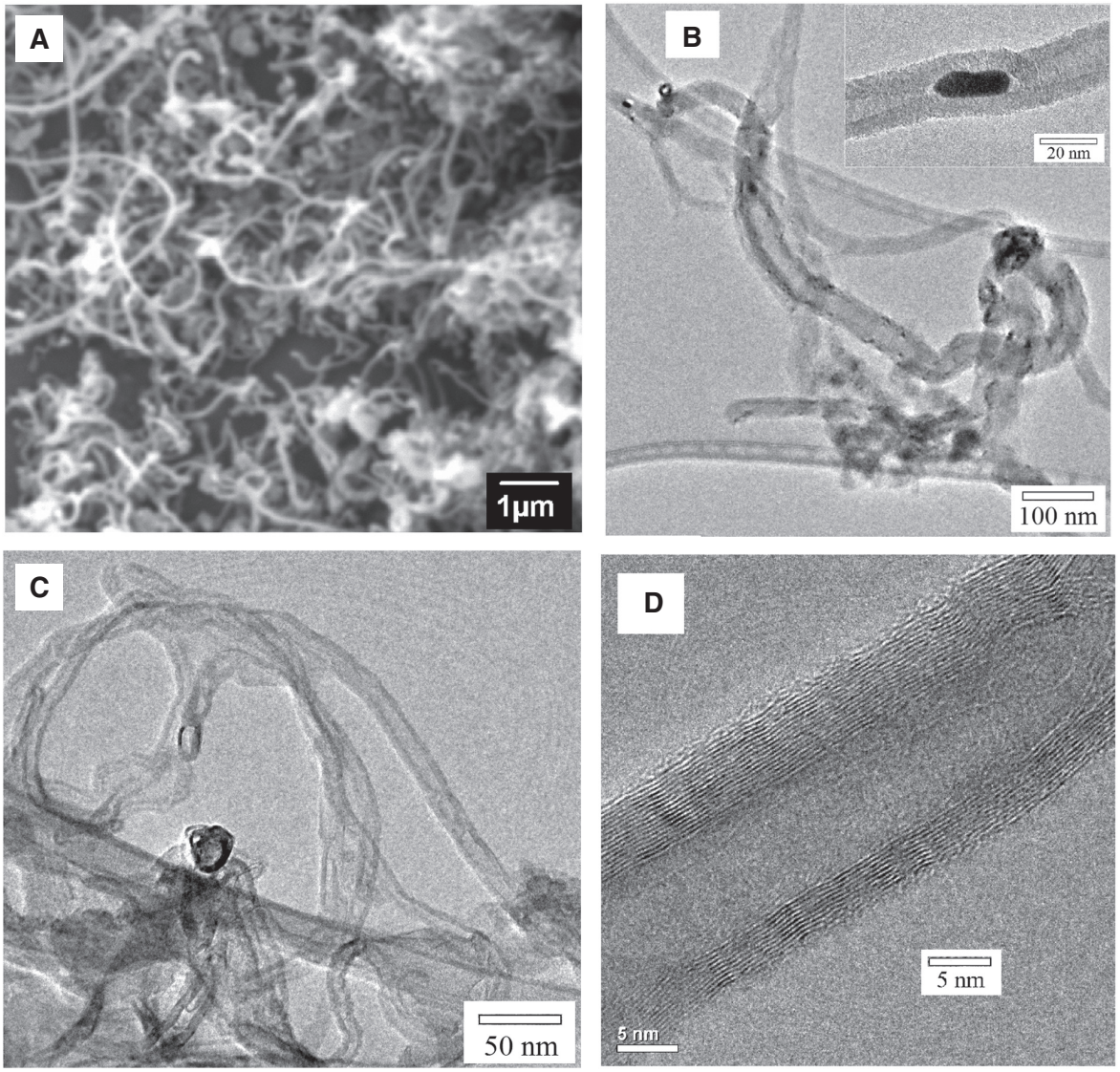

Figure 3: (A, B) Scanning electron microscopy (SEM) and electron microscopy (TEM) microstructures of the as-synthesized carbon nanotubes (CNT); the inset in B shows catalyst nanoparticle inside CNT and (C, D) TEM and high-resolution TEM (HR-TEM) results of the CNT after purification and covalent functionalization.

CNT structure, as well as disruption of the outermost and underlying graphene sheets making up the CNT sidewalls, is also confirmed by Wepasnick et al. [34].

The information regarding the composition and the effect of functionalization treatment thereof on the CNTs was deduced from XRD, TGA/DTA, Raman spectroscopy and FTIR studies, as showcased in Figure 4. The X-ray diffraction pattern of the as-produced CNT revealed their graphitic nature via the presence of highly intense, sharp peaks at 2θ values that correspond to (002), (100) and (101) crystallographic planes [35]. An increase in the peak width and reduced intensities of the diffraction peaks (except for the most intense peak) demonstrate a decline in the crystallographic quality of the CNT upon attachment of the -COOH group. The investigation of the CNT thermal properties (Figure 4B) points towards a progressive decline in the temperature, indicative of the onset of thermal decomposition, with an increase in the number of functional groups attached to the CNT. The attachment of different functional groups is noticed to adversely affect thermal stability of the CNT, which in turn, depends on the type and number of functional groups. While pristine CNT exhibit the maximum degree of thermal stability until 550°C, the temperature representing the onset of thermal degradation significantly drops upon functionalization with carboxylic, acyl and amine groups, primarily due to structural damage to the outermost nanotubes surface and generation of structural defects [36]. Although incorporation of any CNT type (pristine or functionalized) into the epoxy matrix causes improvement in the thermal stability of the resulting nanocomposites, maximum enhancement in thermal properties is seen upon addition of pristine CNTs. Nevertheless, the beneficial effect of CNT incorporation is primarily due to strong interfacial adhesion and homogeneous dispersion in the matrix.

The Raman spectra of the pristine and acid treated (HCl and H_2SO_4/HNO_3 solution) CNT are presented in Figure 4C. It is evident that CNT exhibit the presence of D (disorder) and G (graphite) bands at 1356 cm^{-1} and 1586 cm^{-1}, respectively. While the former is attributed to the disorder-induced vibrations of C-C bonds, the latter is related to the C-C carbon material frequency with a sp^2

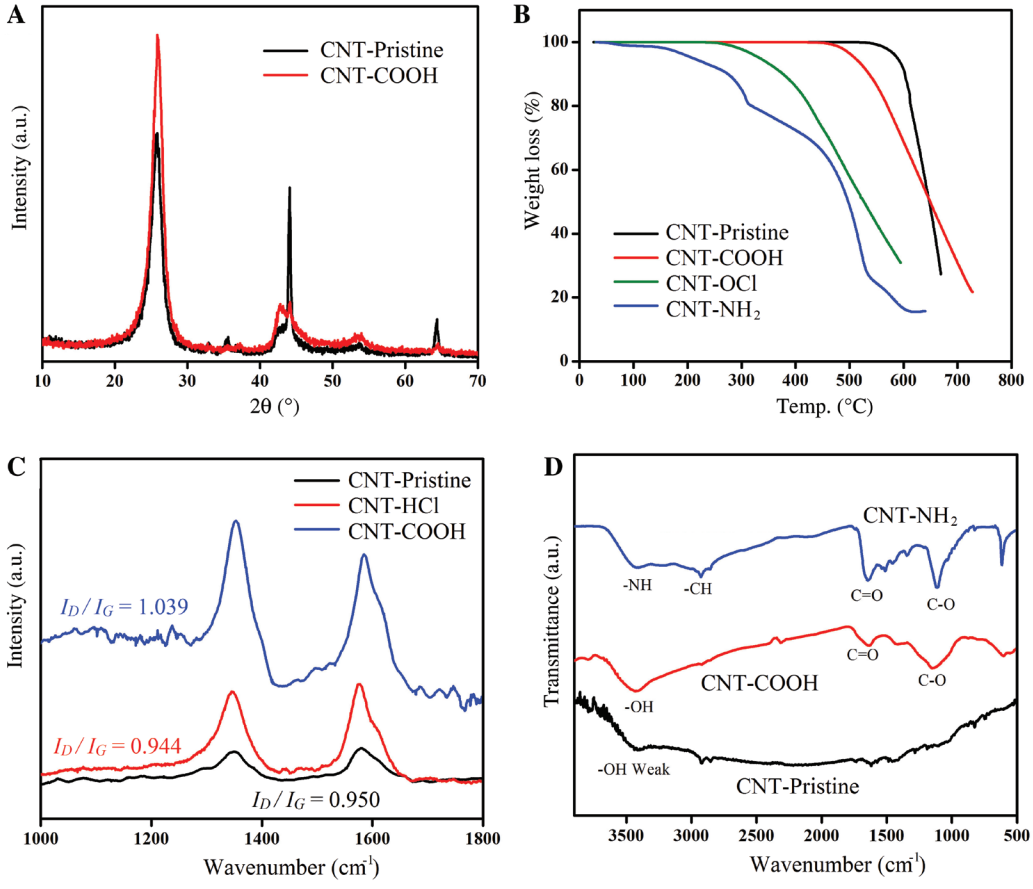

Figure 4: Characterization studies of the as-produced [carbon nanotube (CNT)-pristine] and functionalized (CNT-COOH, CNT-NH_2) CNTs: (A) X-ray diffraction patterns; (B) thermogravimetric analysis; (C) Raman spectra; and (D) Fourier transform infrared spectroscopy studies.

orbital structure [37]. The D band appears due to the presence of amorphous or disordered carbon in the CNT. Generally, the value of intensity ratio of the D and G bands to be <1 implies growth of high quality CNT [38]. From the respective I_D/I_G values given for pristine-, HCl-treated and H_2SO_4/HNO_3 mixture solution treated CNTs shown in Figure 4C, it is noticed that while the values are almost similar for the former two types (pristine- and HCl-treated) suggesting high CNT quality, there is relatively little extent of defects generation on CNT surface besides removal of the catalyst nanoparticles. This finding coincides very well with the microstructural analysis performed using HR-TEM, where CNT treatment with HCl successfully removed catalyst nanoparticles and did not cause any disruption in shell structure or on the CNT surface. Further treatment with H_2SO_4/HNO_3 mixture solution, however, causes an increase in the I_D/I_G value to 1.03, which confirms that such treatment generates surface defects with an associated increase in the D band intensity. During acidic treatment, the functional groups get attached to the CNT outer shells beside generation of physical defects on the surface. The defects so produced cause disorder in the CNT structure to a certain extent, thus giving rise to an increase in the intensity of the D band [39].

The FTIR spectra of the pristine and functionalized CNTs are shown in Figure 4D. While the absorption band positioned at 1618 cm^{-1} can be assigned to the C=C stretching vibrations mode associated with the CNT sidewalls, the band located at 2917 cm^{-1} is due to in-plane vibrations of the C-H bond in the CNTs. The vibrations characteristic of these chemical bonds confirms the aromatic structure of the CNTs [40]. The band at 3400 cm^{-1}, seen in the case of pristine CNT, is due to adsorbed water molecules as moisture. Two additional bands, observed in carboxylic functionalized CNT at 3400 cm^{-1} and 1634 cm^{-1}, can be attributed to the hydroxyl (-OH) and carboxyl (C=O) groups, respectively, because of stretching vibrations of -OH and C=O groups. The peak observed at 1110 cm^{-1} corresponds to the C-O bond. The amine functionalization is confirmed by two specific bands originated by amine groups at 3417 cm^{-1} and 1621 cm^{-1} that replace the -OH and C=O groups, respectively. Thus, FTIR data confirms CNT functionalization through defect and covalent chemistry.

The CNT dispersion studies were performed using different liquid media. The dispersion stability was assessed by measuring the time it takes by CNT (pristine and functionalized) to completely settle down in the liquid medium. Regardless of the CNT type, the dispersions were more stable in water than acetone. It was also observed that CNT-COOH exhibits superior dispersion characteristics in water, whereas CNT-NH_2 is more dispersible in acetone.

3.3 Mechanical testing of Ep/CNT nanocomposites

From tensile testing of the notch-free and notched samples, the values of ultimate tensile strength (σ_{TS}) and elastic modulus (E) for different epoxy/CNT nanocomposites were determined. For both notch-free and notched specimens, the data is plotted against CNT loading (wt%), as presented in Figures 5 and 6, respectively. For neat epoxy, introduction of a defect, such as a notch, causes a drop in the tensile strength (σ_{TS}) by more than a factor of 3. Upon loading with different CNT types, the same trend in the change in σ_{TS} values is noticed for nanocomposites reinforced with CNT-NH_2 or CNT-COOH, where the value

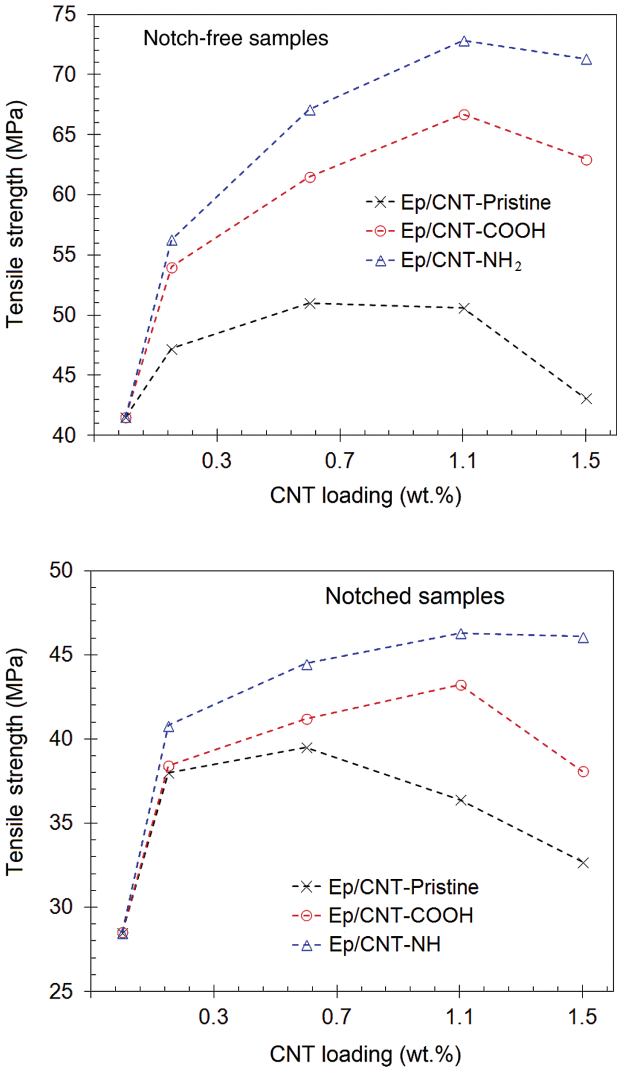

Figure 5: Tensile strength data as a function of carbon nanotube (CNT) wt% for the test specimens made of different epoxy (Ep)/CNT nanocomposites (A) without any pre-crack and (B) with a notch in the form of 0.3 mm pre-crack.

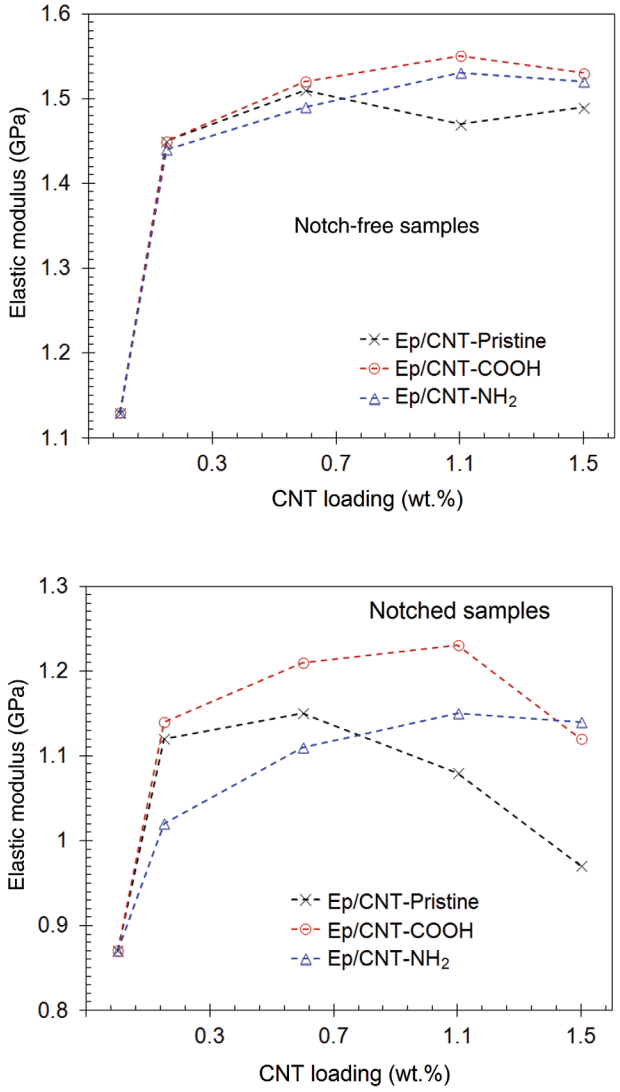

Figure 6: Elastic modulus of the epoxy (Ep)/carbon nanotube (CNT) nanocomposites with different CNT weight (A) without any pre-crack and (B) with a 0.3 mm pre-crack.

maximizes upon reinforcement with 1.1 wt% of the nanotubes, followed by a slight decrease upon further loading to 1.5 wt%. By contrast, addition of 0.6 wt% pristine CNT leads to a maximum tensile strength value followed by a drop upon greater loading levels. The reduction in σ_{TS} value, after it has attained a maximum value, is presumably due to CNT agglomeration and inhomogeneous dispersion in the matrix. The maximum percent increase in the σ_{TS} value, for nanocomposites prepared with different CNT types, in is the following order: 1.1 CNT-NH_2 (+73%)>1.1 CNT-COOH (+67%)>0.6 CNT-pristine (+51%). A similar trend is seen in the notched samples (Figure 5B), although the σ_{TS} values are lower than in notch-free samples. Nevertheless, incorporation of as little as 0.6 wt% CNT, whether pristine or functionalized, can improve tensile strength of the notched specimens to become equivalent or greater than that of notch-free epoxy samples.

The elastic modulus values for different nanocomposites are presented graphically in Figure 6. The elastic modulus values for the notched and notch-free specimens are 0.87 GPa and 1.13 GPa, respectively. For both sample types, the maximum increase is noticed in the case of 1.1 wt% CNT-COOH reinforcement, indicative of efficient load transfer from the matrix to the CNT while in tension, owing to better interfacial strength and good dispersion within the epoxy matrix. As compared to neat epoxy, the percent increase in the 1.1 wt% CNT-COOH reinforced epoxy nanocomposite is on the order of 37% and 41%, respectively, for notched and notch-free specimens. The presence of a notch acts as a stress concentration site for crack initiation and its subsequent propagation. The sample failure in the vicinity of the crack also validated the aforementioned behavior.

Comparison of the tensile testing data presented in this paper with some published results is made in Table 1. The values of elastic modulus and tensile strength are listed along with percent change as compared to those for neat epoxy in parentheses. The present study offers insights into the CNT reinforcing effect on epoxy with three distinct perspectives: (i) the experimental procedure is quite simple and brief in contrast with reported studies; (ii) reasonable degrees of enhancement in both elastic modulus and tensile strength are achieved while significant improvement in either of these is reported

Table 1: Effect of covalent treatment of carbon nanotube (CNT) on mechanical properties of epoxy nanocomposites.

Sample description	Tensile modulus (GPa)	Tensile strength (MPa)	Reference
Defect-free specimens			
No filler	1.13	41.5	This work
Untreated CNT (0.6)	1.51 (+33.6)	51 (+22.9)	
Acid treated (1.1)	1.55 (+37.2)	66.7 (+60.7)	
Amine treated (1.1)	1.53 (35.4)	72.8 (75.4)	
Notched specimens			
No filler	0.87	28.5	This work
Untreated CNT (0.6)	1.15 (+32.2)	39.5 (+38.6)	
Acid treated (1.1)	1.23 (+41.4)	43.2 (+51.6)	
Amine treated (1.1)	1.15 (+32.2)	46.3 (+62.5)	
Acid treated, plasma oxidized			
No filler	1.21	26	[41]
Untreated CNT (1.0)	1.38 (+14)	42 (+62)	
Acid treated (1.0)	1.22	44 (+69)	
Amine treated (1.0)	1.23	47 (+81)	
Acid treated (0.1–1.0)	+90	+45	[42]

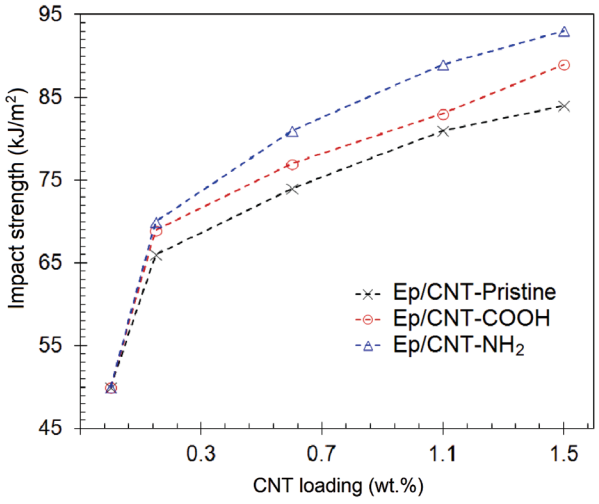

Figure 7: Toughness of the neat and carbon nanotube (CNT)-reinforced epoxy nanocomposites containing pristine or functionalized CNT by 0.15, 0.6, 1.1 and 1.50 wt%.

in literature; and (iii) the effect of a structural defect in the form of a notch is taken into consideration, showing improved properties compared to neat epoxy.

The Charpy impact tests were used to assess incorporation of different CNT types on toughness of the resulting nanocomposites. Figure 7 presents energy absorbed by the sample before fracture as a function of CNT wt% in the nanocomposites for pristine and functionalized CNT. Thus, the advantages of strong interfacial adhesion due to defect structure and functional group attached to the CNT surface, uniform CNT dispersion within the matrix with fewer tendencies to form agglomerates or entangled networks are exploited to obtain superior toughness against impact loading. While all the nanocomposite formulations exhibited a progressive increase in toughness for the range of CNT wt% values explored, the maximum degree of toughness enhancement, i.e., by 86%, was recorded for 1.5 CNT-NH_2 reinforced nanocomposites. Yaping et al. [43] reported an increase in impact strength by about 80% upon addition of 0.6 wt% CNT-NH_2. More recently, about 58% increase in the value of impact strength was recorded in cyanate ester/epoxy nanocomposites containing 0.5 wt% functionalized CNT [44]. Although further increase in toughness may be possible through CNT addition by >1.5 wt%, the tensile properties will be compromised, as noticed by a decline in the

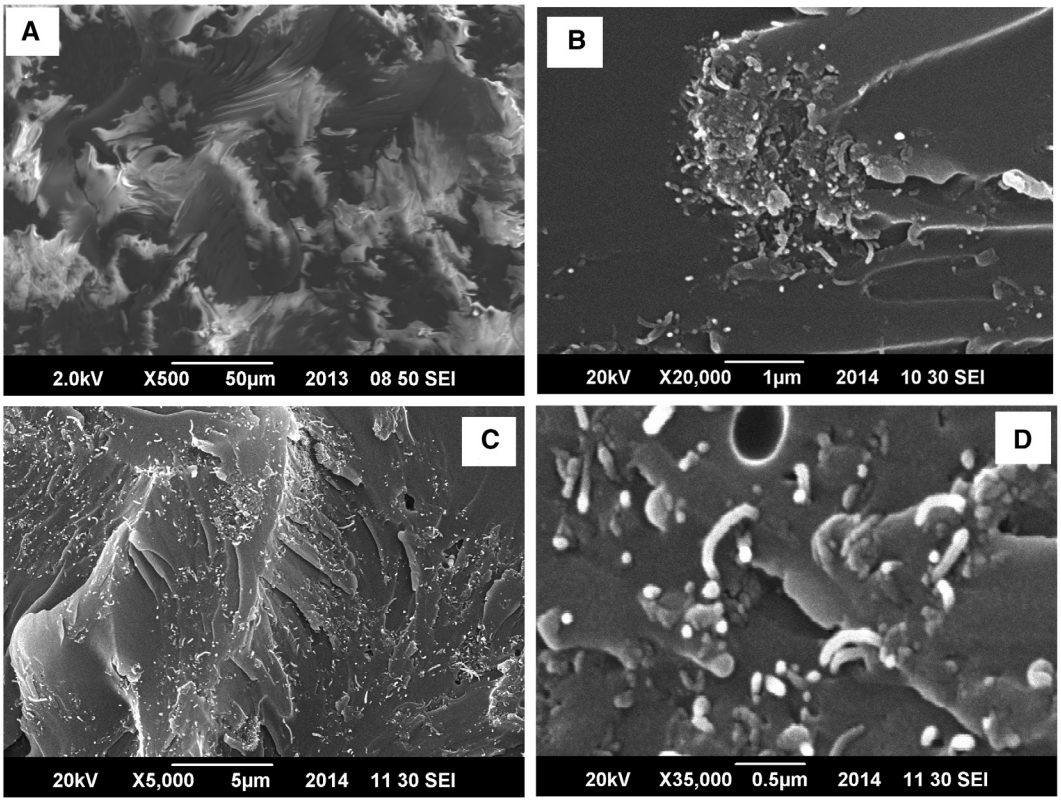

Figure 8: Electron microscope images of the fractured surfaces of different epoxy (Ep)/carbon nanotube (CNT) nanocomposites after impact test (A) and tensile tests (B–D): (A) low magnification view of the Ep/CNT-COOH sample; (B) non-uniform dispersion of CNT-pristine in the epoxy matrix; (C, D) low and high magnification view of the 1.1 Ep/CNT-NH_2 nanocomposites showing CNT dispersion and debonding/pullout from the matrix during testing.

tensile strength and elastic modulus values after reaching a maximum.

The dispersion of different CNT types in the epoxy matrix was assessed through SEM examination of the fractured surfaces of the impact specimens, shown in Figure 8. The low magnification microstructure (Figure 8A) represents cup-and-cone fracture morphology prevalent in the CNT-reinforced epoxy nanocomposites. Distribution of pristine CNT in the matrix is inhomogeneous (Figure 8B), as evident from segregation of CNT in a localized region. Thus, the effectiveness of pristine CNT in the polymer matrix is somehow curtailed due to difficulty in disentanglement during processing and lack of any mechanism to suppress agglomeration. The functionalization treatment leading to the attachment of -NH_2 groups resulted in excellent dispersion, as demonstrated in Figure 8C. During impact loading, the CNT experience debonding and pull-out from the matrix, indicated by short lengths protruding out of the fractured surface (Figure 8D). The fact that the outer diameter of such strands is around 70–80 nm highlights good interfacial bonding of the CNT with the matrix and subsequently efficient load transfer. The homogeneous distribution and good adhesion with the matrix result in the maximum degree of improvement in the tensile and impact strength of the CNT-NH_2 reinforced nanocomposites.

4 Conclusions

Using the co-precipitate method and CTAB as surfactant, $NiFe_2O_4$ nanoparticles with narrow size distribution can be produced. Through gas mixture flow of precursor hydrocarbon C_2H_2 and argon as diluting agent in 1:9 (sccm) at 680°C, multi-walled CNTs were produced via a catalytic action of $NiFe_2O_4$ nanoparticles. The C_2H_2:argon flow ratio plays a critical role, as suboptimal growth conditions cause complete encapsulation of the catalyst nanoparticle surface, thus cutting off the carbon source and terminating the CNT growth. Attachment of different functional groups such as -COOH or -NH_2 via defect and covalent functionalization causes surface modification of the nanotubes, leading to changes in thermal properties and promotes homogeneous dispersion with reduced tendency to form agglomerates. Whether in pristine form or after functionalization treatment, the CNT reinforcement of the epoxy matrix causes improvement in mechanical properties due to efficient load transfer to the nanotubes. Upon addition of 1.1 wt% CNT-COOH (or CNT-NH_2), the values of elastic modulus and tensile strength maximize from 1.13 GPa and 41.5 MPa for the neat epoxy, to 1.55 GPa (or 1.53 GPa) and 72.8 MPa (or 66.7 MPa), respectively, for the resulting nanocomposites. The use of CNT as a filler also offsets the adverse effects of a structural weakness such as a notch or crack in the specimen, as superior tensile properties were recorded in notched nanocomposite samples compared to those for the neat epoxy. Several factors, including CNT purification and surface modification, strong interfacial bonding between the epoxy matrix and the CNT, homogeneous dispersion with little or no CNT entanglement and subsequently, good load bearing characteristics during mechanical testing, contribute towards development of stronger and more tough CNT-reinforced nanocomposites.

Acknowledgments: The authors are grateful to Nicolas Gautier from Jean Rouxel Institut des Matériaux, Nantes, France for technical assistance with HR-TEM. The authors thankfully acknowledge a financial grant from the National University of Science and Technology, Pakistan. The authors would like to extend their sincere appreciation to the Deanship of Scientific Research at King Saud University for funding of this research through the Research Group Project No. RGP-VPP-283.

References

[1] Han J. In *Carbon Nanotubes: Science and Applications*, Meyyappan M, Ed., CRC Press, FL, USA: 2004, pp. 2–21.
[2] Laird ED, Hood MA, Li CY. In *Carbon Nanomaterials*, Gogotsi Y, Presser V, Eds., CRC Press, FL, USA, LLC: 2014, pp. 135–186.
[3] Berhan L, Yi Y, Sastry A, Munoz E, Selvidge M, Baughman R. *J. Appl. Phys*. 2044, 95, 4335.
[4] Chang L, Hui-Ming C. *J. Phys. D: Appl. Phys*. 2005, 38, R231.
[5] Melechko AV, Merkulov VI, McKnight TE, Guillorn MA, Klein KL, Lowndes DH, Simpson ML. *J. Appl. Phys*. 2005, 97, 041301.
[6] Sarangi D, Hierold C, Karimi A. *Fullerenes, Nanotubes, Carbon Nanostruct*. 2005, 13, 243–253.
[7] Makris TD, Giorgi L, Giorgi R, Lisi N, Salernitano E. *Diamond Relat. Mater*. 2005, 14, 815–819.
[8] Ago H, Imamura S, Okazaki T, Saito T, Yumura M, Tsuji M. *J. Phys. Chem. B* 2005, 109, 10035–10041.
[9] Jang YT, Ahn J-H, Lee Y-H, Ju B-K. *Chem. Phys. Lett*. 2003, 372, 745–749.
[10] Mauron P, Emmenegger C, Sudan P, Wenger P, Rentsch S, Züttel A. *Diamond Relat. Mater*. 2003, 12, 780–785.
[11] Cui H, Eres G, Howe JY, Puretkzy A, Varela M, Geohegan DB, Lowndes DH. *Chem. Phys. Lett*. 2003, 374, 222–228.
[12] Magrez A, Seo JW, Mikó C, Hernádi K, Forró L. *J. Phys. Chem. B* 2005, 109, 10087–10091.
[13] Morjan RE, Maltsev V, Nerushev O, Yao Y, Falk LKL, Campbell EEB. *Chem. Phys. Lett*. 2004, 383, 385–390.

[14] Geohegan DB, Puretzky AA, Ivanov IN, Jesse S, Eres G, Howe JY. *Appl. Phys. Lett.* 2003, 83, 1851.
[15] Zhang H, Liang E, Ding P, Chao M. *Phys. B* 2003, 337, 10.
[16] Taylor C, Cavicchi RE, Montgomery CB, Turner S. *Nanotechnology* 2004, 15, 62.
[17] Kukovecz Á, Méhn D, Nemes-Nagy E, Szabó R, Kiricsi I. *Carbon* 2005, 43, 2842–2849.
[18] Singh C, Shaffer MSP, Windle AH. *Carbon* 2003, 41, 359.
[19] Afrin R, Khaliq J, Islam M, Gul IH, Bhatti AS, Manzoor U. *Sensors Actuators A* 2012, 187, 73–78.
[20] Kitano H, Tachimoto K, Anraku Y. *J. Colloid Interface Sci.* 2007, 306, 28–33.
[21] Shen J, Huang W, Wu L, Hu Y, Ye M. *Mater. Sci. Eng. A* 2007, 464, 151–156.
[22] Men XH, Zhang ZZ, Song HJ, Wang K, Jiang W. *Compos. Sci. Technol.* 2008, 68, 1042–1049.
[23] Ye Y, Chen H, Wu J, Ye L. *Polymer* 2007, 48, 6426–6433.
[24] Fidelus J, Wiesel E, Gojny F, Schulte K, Wagner H. *Composites A* 2005, 36, 1555.
[25] Liu L-Q, Wagner HD. *Compos. Interfaces* 2007, 14, 285–297.
[26] Spitalsky Z, Tasis D, Papagelis K, Galiotis C. *Prog. Polym. Sci.* 2010, 35, 357–401.
[27] Gojny FH, Wichmann MH, Fiedler B, Schulte K. *Compos. Sci. Technol.* 2005, 65, 2300–2313.
[28] Hameed A, Islam M, Ahmad I, Mahmood N, Saeed S, Javed H. *Polym. Composites* 2014. doi:10.1002/pc.23097.
[29] Mahmood N, Islam M, Hameed A, Saeed S. *Polymers* 2013, 5, 1380–1391.
[30] Ogasawara T, Moon S-Y, Inoue Y, Shimamura Y. *Compos. Sci. Technol.* 2011, 71, 1826–1833.
[31] Nguyen T-D, Do T-O. *Size- and Shape-Controlled Synthesis of Monodisperse Metal Oxide and Mixed Oxide Nanocrystals, Nanocrystal*, Masuda Y, Ed., ISBN: 978-953-307-199-2, InTech, Croatia, 2011.
[32] Dong Q, Yin S, Guo CS, Li HH, Kumada N, Takei T, Yonesaki Y, Kinomura N, Sato T. *J. Phys.: Conference Series* 2012, 339, 012004.
[33] Nikolic AS, Jovic N, Rogan J, Kremenovic A, Ristic M, Meden A, Antic B. *Ceram. Int.* 2013, 39, 6681–6688.
[34] Wepasnick KA, Smith BA, Schrote KE, Wilson HK, Diegelmann SR, Fairbrother DH. *Carbon* 2011, 49, 24–36.
[35] Roh HS, Potdar HS, Jun KW, Kim JW, Oh YS. *Appl. Catal., A* 2004, 276, 231–239.
[36] Titus E, Ali N, Cabral G, Gracio J, Babu PR, Jackson M. *J. Mater. Eng. Performance* 2006, 15, 182–186.
[37] Zhang D, Shi L, Fang J, Li X, Dai K. *Mater. Lett.* 2005, 59, 4044–4047.
[38] Tuinstra F, Koenig JL. *J. Chem. Phys.* 1970, 53, 1126.
[39] Osorio AG, Silveira ICL, Bueno VL. Bergmann CP. *Appl. Surf. Sci.* 2008, 255, 2485–2489.
[40] Chen GX, Kim H-S, Park BH, Yoon J-S. *Polymer* 2006, 47, 4760–4767.
[41] Kim JA, Seong DG, Kang TJ, Youn JR. *Carbon* 2006, 44, 1898–1905.
[42] Zou W, Du Z-J, Liu Y-X, Yang X, Li H-Q, Zhang C. *Compos. Sci. Technol.* 2008, 68, 3259–3264.
[43] Yaping Z, Aibo Z, Qinghua C, Jiaoxia Z, Rongchang N. *Mater. Sci. Eng. A* 2006, 435–436, 145–149.
[44] Li J, Wu Z, Huang C, Liu H, Huang R, Li K. *Compos. Sci. Technol.* 2014, 90, 166–173.